

Development of 400-μW cryogen-free dilution refrigerators for quantum experiments

Xiang Guan(关翔), Jie Fan(樊洁), Yong-Bo Bian(边勇波), Zhi-Gang Cheng(程智刚), and Zhong-Qing Ji(姬忠庆)
Citation: Chin. Phys. B, 2024, 33 (**7**): 070701. DOI: 10.1088/1674-1056/ad3b87
Journal homepage: http://cpb.iphy.ac.cn; http://iopscience.iop.org/cpb

What follows is a list of articles you may be interested in

Development of a cryogen-free dilution refrigerator

Zhongqing Ji(姬忠庆), Jie Fan(樊洁), Jing Dong(董靖), Yongbo Bian(边勇波), and Zhi-Gang Cheng(程智刚)
Chin. Phys. B, 2022, 31 (**12**): 120703. DOI: 10.1088/1674-1056/ac9042

Low-temperature environments for quantum computation and quantum simulation

Hailong Fu(付海龙), Pengjie Wang(王鹏捷), Zhenhai Hu(胡禛海), Yifan Li(李亦璠), and Xi Lin(林熙)
Chin. Phys. B, 2021, 30 (**2**): 020702. DOI: 10.1088/1674-1056/abd762

Sub-millikelvin station at Synergetic Extreme Condition User Facility

Zhi Gang Cheng(程智刚), Jie Fan(樊洁), Xiunian Jing(景秀年), Li Lu(吕力)
Chin. Phys. B, 2018, 27 (**7**): 070702. DOI: 10.1088/1674-1056/27/7/070702

Cryogenic amplifier with low input-referred voltage noise calibrated by shot noise measurement

Wuhao Yang(杨伍昊), Jian Wei(危健)
Chin. Phys. B, 2018, 27 (**6**): 060702. DOI: 10.1088/1674-1056/27/6/060702

4.3 THz quantum-well photodetectors with high detection sensitivity

Zhenzhen Zhang(张真真), Zhanglong Fu(符张龙), Xuguang Guo(郭旭光), Juncheng Cao(曹俊诚)
Chin. Phys. B, 2018, 27 (**3**): 030701. DOI: 10.1088/1674-1056/27/3/030701

INSTRUMENTATION AND MEASUREMENT

Development of 400-μW cryogen-free dilution refrigerators for quantum experiments

Xiang Guan(关翔)[1], Jie Fan(樊洁)[1], Yong-Bo Bian(边勇波)[1], Zhi-Gang Cheng(程智刚)[1,2], and Zhong-Qing Ji(姬忠庆)[1,†]

[1] *Institute of Physics, Chinese Academy of Sciences, Beijing* 100190, *China*
[2] *School of Physical Sciences, University of Chinese Academy of Sciences, Beijing* 100190, *China*

(Received 5 February 2024; revised manuscript received 16 March 2024; accepted manuscript online 7 April 2024)

We have successfully developed cryogen-free dilution refrigerators with medium cooling power that can be applied to quantum experiments. Breakthroughs have been made in some key technologies and components of heat switches and dilution units. Our prototype has been running continuously and stably for more than 100 hours below 10 mK, with a minimum temperature of 7.6 mK and a cooling power of 450 μW at 100 mK. At the same time, we have also made progress in the application of dilution refrigerators, such as quantum computing, low-temperature detector, and magnet integration. These indicators and test results indicate good prospects for application in physics, astronomy, and quantum information.

Keywords: cryogen-free dilution refrigerator, quantum computing, low-temperature detector, superconducting magnet

PACS: 07.20.Mc, 67.25.–k, 67.30.–n, 67.60.–g **DOI:** 10.1088/1674-1056/ad3b87

1. Background introduction

The dilution refrigerator (DR) is an advanced scientific research instrument that can provide a continuous ultralow temperature environment of around 10 mK. It has important applications in various fields, such as condensed matter physics, materials science, and astronomical exploration, and is also a key component of some quantum computing and quantum sensing systems.

Since the birth of the first DR in 1965, its development has undergone a rapid leap from wet systems to dry systems, and from laboratory prototypes to commercial products.[1] A group of mature DR companies have emerged abroad, such as Bluefors from Finland, Oxford Instruments from the UK, and Leiden Cryogenics from the Netherlands. However, in response to the urgent development needs in the field of quantum computing, many internationally renowned enterprises and research institutions have recently laid out new or large DRs in order to gain an advantage in the fierce competition. For example, in September 2022, IBM launched the world's largest cryogen-free DR, called Goldeneye, which has an experimental volume of 1.5 m^3 and a cooling power of 10 mW@100 mK.[2] The Fermi Laboratory of the US Department of Energy is developing a new generation of DR, called Colossus, which combines large-scale cryogenic refrigeration technology with the existing mature dilution units, and will have an experimental volume of approximately 5 m^3 and a cooling power of 300–500 μW@20 mK. This so-called world's largest DR is expected to be operational by 2025.[3,4]

China has experienced a nearly 20-year technological gap in the field of DR. In recent years, the Institute of Physics of Chinese Academy of Sciences, the Pride Cryogenics in Nanjing, the 16th Research Institute of China Electronics Technology Corporation, the Anhui University and some other teams have been conducting relevant research. We were the first to develop a prototype DR that can achieve a temperature of 10.9 mK in June 2021, and the others have also made some breakthroughs.[5–9] With these advances, some commercial DR companies have just emerged in China, such as Physike Technology, ZL Cryogenics, QuantumCTek, Origin Quantum, etc. However, in general, the research and development of DR in China are still in its early stages, which is reflected in the lack of mature commercial products, the absence of large-scale DRs with a cooling power larger than 1 mW (at 100 mK), and the fact that existing refrigerators have not yet undergone long-term application tests. In addition, some key components, such as pulse tube (PT) refrigerator and ultralow temperature thermometer, also need to be developed further. In this situation, we carried out the project of developing a 400-μW cryogen-free DR. This paper will provide a detailed introduction from multiple aspects, including technical principles and system architecture, key components, experimental results, and some application tests.

2. Technical principles and system architecture

The core principle of dilution refrigeration lies in the endothermic process that occurs when ^{3}He atoms transfer from

[†]Corresponding author. E-mail: zji@iphy.ac.cn

© 2024 Chinese Physical Society and IOP Publishing Ltd

the concentrated phase solution (a mixture with a high ^{3}He content) to the dilute phase solution (a mixture with a low ^{3}He content) under the condition where ^{3}He and ^{4}He mixed liquids are separated (< 0.87 K). Depending on the precooling method used, DRs can be categorized into wet systems and dry systems. Wet systems rely on liquid helium for precooling, whereas dry systems utilize small mechanical refrigerators (e.g., GM refrigerator or PT refrigerator) for precooling instead of liquid helium. Hence, they are also known as cryogen-free DRs, which consume almost no liquid helium and are more convenient to use. They represent the mainstream products[10] currently and are the main focus of our research in this paper.

The specific working principle of the cryogen-free DR is depicted in Fig. 1. Under the cooling effect of the mechanical refrigerator's cold head, the first and second stage cold plates can reach temperatures of approximately 40 K and 3 K, respectively. In the pumping line, the mixture gas, primarily composed of ^{3}He, evaporates from the still under the action of an external pump group. The extracted ^{3}He then returns through the return line, forming a cycle. This returned gas passes through heat exchange with the first and second stage cold plates before entering the JT condenser, where it is completely liquefied. Below the still stage cold plate, there are a counter-flow heat exchanger (CHE) and a step heat exchanger (SHE) placed sequentially. The concentrated phase solution flowing towards the mixing chamber (MC) is precooled by the dilute phase solution exiting the mixing chamber in the heat exchangers, causing its temperature to gradually decrease. Finally, at the phase separation interface in the MC, ^{3}He atoms from the concentrated phase continuously enter the dilute phase solution, generating a cooling effect that can reach temperatures as low as 10 mK. To achieve the aforementioned principles, a cryogen-free DR typically includes four major components: a precooling system, a dilution unit, a gas management system, and a temperature measurement system.

The precooling system mainly includes a mechanical refrigerator and heat switch components, providing the necessary conditions for dilution refrigeration. It is also related to the overall cooling rate and the realization of core performance indicators. In this project, we prioritized the use of a two-stage PT refrigerator with a cooling power of 1.5 W at 4.2 K as cold source for precooling. At the same time, experiments with precooling schemes based on GM refrigerator were also conducted. We have verified that a cryogen-free DR precooled by a GM refrigerator can also reach temperatures on the order of 10 mK, provided that the system is adequately vibration-damped. The heat switch components are used for cryogenic thermal management in the DR system. In the early stage of precooling, the lower stage cold plate needs to establish a thermal connection with the second stage cold plate through heat switches. After being precooled to about 10 K, the thermal connection must be disconnected to reduce heat leakage from the high-temperature zone to the low-temperature zone, allowing for lower temperatures to be achieved through evaporative cooling and dilution refrigeration. During the implementation of this project, we initially adopted a relatively simple mechanical heat switch to fulfill this function, and then explored some other heat switch schemes.

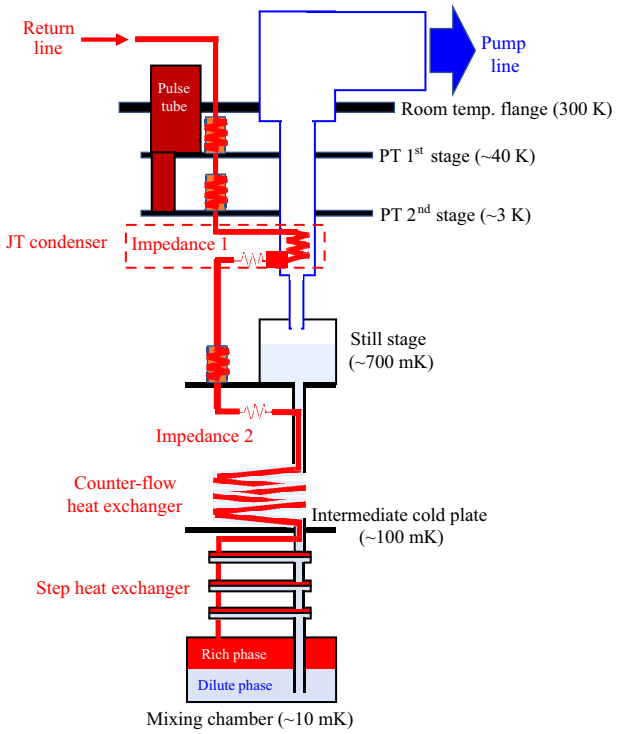


Fig. 1. Schematic diagram of a cryogen-free DR.[11]

The dilution unit is the core functional module of DR that can achieve some important processes, from helium liquefaction to dilution refrigeration. It mainly includes JT condenser, flow impedance, still, CHE, SHE, and MC. In this project, the design, process, manufacturing, and test of the dilution unit were all independently completed by us. The detailed structure and principles of these components were introduced in our early paper.[11] In the following text, we will only introduce some key components or technologies in this development.

The gas management system is used to store, control, filter, and circulate gases in the DR, mainly including gas tanks, valves, cold traps, pump groups, etc. In this project, we have developed an intelligent gas control cabinet based on LabVIEW, which can monitor the operation of the system in real time and also achieve automatic operation.

The temperature measurement system is used to monitor the temperature of each stage of the DR, which includes thermometers, temperature measurement leads, acquisition and controller (AC bridge), etc. We have used different types of resistance thermometers in different temperature zones. The RX-102B thermometer used for measuring the MC was calibrated by Lakeshore company.

3. Key components

3.1. Heat switch for high efficiency precooling

In the first generation of our DR, we reported on a composite type of heat switch.[11] Above the still stage cold plate, a mechanical heat switch was used. While below the still stage, thermal connection and insulation were achieved by relying on the change in thermal conductivity of aluminum rods from room temperature to low temperature, which was referred to as a passive heat switch. The principle of the passive heat switch is simple, and the low thermal conductivity of aluminum at low temperatures ensures minimal heat leakage, but this extends the precooling time. In this work, we have adopted mechanical heat switch at all cold plate stages, namely, an improved multistage mechanical heat switch. Its physical photo is shown in Fig. 2. The theoretical "switching ratio" of this type heat switch approaches infinity, and it can precool the various stages of cold plates to the low temperatures of 3–4 K. However, its main disadvantage lies in the relatively low reliability of multistage linkage at low temperatures. If not handled properly, it can lead to a very slow precooling rate or failure to completely disconnect at low temperatures, causing the temperature to deviate from the normal range. To address this, we have made improvements in several aspects. For example, we used a pneumatic valve and springs to control the ON and OFF states of the heat switch. In order to improve the thermal conductivity in the ON state, each stage of the heat switch was ensured to have a good contact surface. The pneumatic valve has been determined to be able to apply continuous and sufficient pressure to maintain good contact between the levels, even when materials contract at low temperatures. On the other hand, to ensure the complete disconnection of the heat switch when necessary, beryllium copper springs have become our preferred choice. Additionally, the low-temperature shrinkage properties of the materials were also considered in our design to prevent the heat switch from getting stuck during operation. The mechanical heat switch developed in this project has a conductor diameter of about 12 mm. Finally, the still stage cold plate can be cooled to 4 K in about 36 hours, as shown in Fig. 3. The overall precooling rate is greatly improved compared with the prototype.

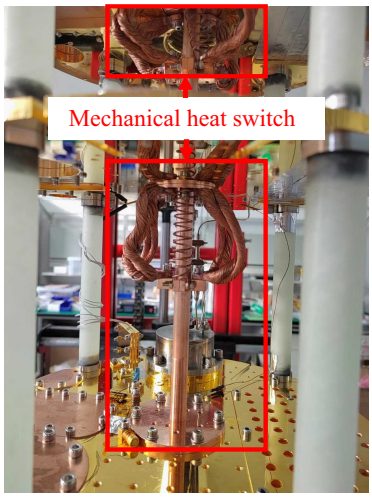


Fig. 2. The mechanical heat switch developed in this project.

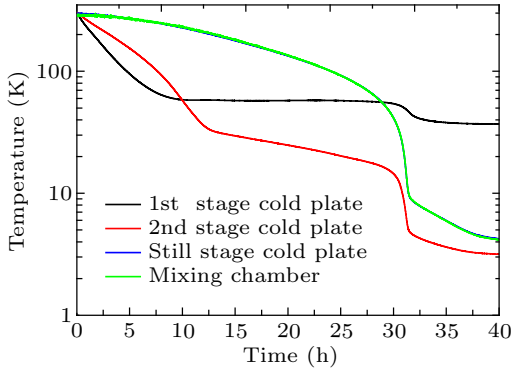


Fig. 3. The temperature changes of different cold plates during precooling.

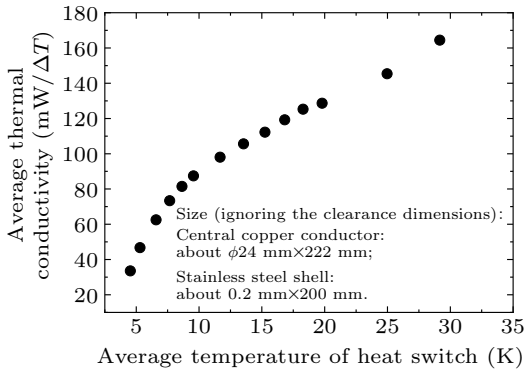


Fig. 4. The typical thermal conductivity of our gas gap heat switch.

In addition to the mechanical heat switch, we have also recently developed a gas gap heat switch based on the principle of materials' low-temperature linear expansion. The conductor diameter of the gas gap heat switch that we designed is 24 mm, with the inner diameter of the stainless shell being 28 mm and a wall thickness of 0.2 mm. Disregarding the gap size (on the order of tens of micrometers), the height of the gas gap heat switch corresponds to the spacing of the cold plate. The typical thermal conductivity test results of a set of switches (approximately 222 mm in height) in the ON state are shown in Fig. 4, and its thermal conductivity in the OFF state is about 0.1 mW/K. So, it can be known that the heat switch has achieved a switching ratio of more than 1000 in the temperature range of 4–40 K in a single test. For a DR equipped with six gas gap heat switches with performance similar to those shown in Fig. 4, its cold plates at all levels can be cooled down to about 10 K in 24 hours, which is close to the level of a commercial refrigerator.[12] With the research on a variety of heat switch technologies, our refrigerator will achieve efficient precooling in the near future.

3.2. Flow impedance

The flow impedance mainly affects the osmotic pressure distribution within the internal pipeline, which in turn influences the condensation rate and steady flow of the system. Our research has found that for a given system, reducing the flow impedance appropriately can accelerate the condensation rate. However, if the flow impedance is too low, the flow will increase under steady-state conditions, which is not conducive to achieving the minimum temperature. The setting of the flow impedance needs to be adjusted according to the state of the system. We followed the method described in Ref. [13] to make, measure, and calculate it. The form of flow impedance used in this project is shown in Fig. 5. Its main body is a capillary tube inserted with stainless steel wire, with both ends connected to the pipeline through VCR connectors. The numerical value of the flow impedance can be changed by adjusting the length or diameter of the stainless wire. The main impedance used in this project is about 6×10^{10} cm^{-3}. Under its action, when the pressure at the return line is about 800 mbar, the pressure rise rate at the pump line is about 0.005–0.006 mbar/min (at room temperature).

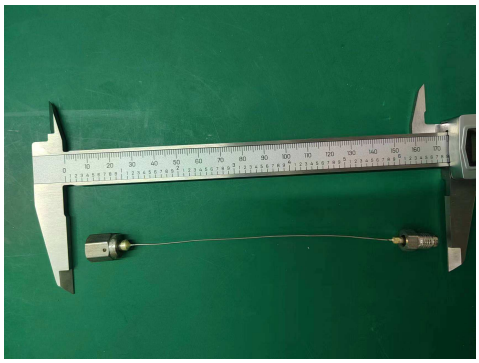


Fig. 5. The flow impedance produced in this project.

3.3. Ultralow temperature heat exchanger

The concentrated phase liquid flowing out of the still requires a series of heat exchanges to achieve further cooling. The thermodynamic equations of ultralow temperature heat exchanger are given below:

$$-A_{\rm c}\frac{\rm d}{{\rm d}x}\left(k_{\rm c}\frac{{\rm d}T_{\rm c}}{{\rm d}x}\right)-\frac{128\eta_{\rm c}\dot{n}^2V_{\rm c}^2}{\pi D_{\rm c}^4}+E\left(T_{\rm c}^4-T_{\rm d}^4\right)=-\dot{n}C_{\rm c}\frac{{\rm d}T_{\rm c}}{{\rm d}x}, \tag{1}$$

$$A_{\rm d}\frac{\rm d}{{\rm d}x}\left(k_{\rm d}\frac{{\rm d}T_{\rm d}}{{\rm d}x}\right)+\frac{128\eta_{\rm d}\dot{n}^2V_{\rm d}^2}{\pi D_{\rm d}^4}+E\left(T_{\rm c}^4-T_{\rm d}^4\right)=-\dot{n}C_{\rm d}\frac{{\rm d}T_{\rm d}}{{\rm d}x}. \tag{2}$$

Here, the first to fourth terms (from the left to the right of the equal sign) describe the heat conduction along the flow direction, the viscous heating, the heat transfer between concentrated and dilute solutions perpendicular to the flow direction (Kapitza term), and the enthalpy change of the solution, respectively. The subscript $j=$ c, d labels the concentrated and dilute phases, respectively. Here, A is the effective cross section area for liquid. The viscous term is specifically given by $128\eta_j\dot{n}^2V_j^2/(\pi D_j^4)$ (where η, D, and V are viscosity, hydraulic diameter of the flow channel, and molar volume, respectively) when the solution state is assumed to be Poisson's flow under steady-state conditions. Here, the molar volume V is defined by the volume that one mole of ^{3}He atoms occupy. E is a measure of heat conductance between the two phases through thermal boundaries, which scales with the contact perimeter at the cross section and the Kapitza conductivity. As we know, the Kapitza term plays a dominant role in heat transfer, but at the same time the viscous heating and heat conduction can also affect the temperature distribution of the heat exchanger. So, the difficulty in the development of ultralow temperature heat exchanger is to overcome the Kapitza thermal resistance, which is inversely proportional to the third power of temperature, and at the same time to avoid heat leakage and reduce the viscous heating in the channel.

We have developed a mature manufacturing process for a CHE, and have investigated the effects of materials, geometric dimensions, and other factors on its performance experimentally. Using our well-made CHE, the minimum temperature of 48 mK has been achieved, even without using the SHE. For the SHE, we mainly developed it in the form of sintered silver powder. The structural design, welding process, quality of silver powder itself, and sintering process all have important impacts on its performance. In the implementation process of this project, we made a lot of attempts on the silver powder heat exchanger in the form of a "sandwich" structure. The argon arc welding process used can basically avoid the phenomenon of super leak at low temperatures. The purchased silver powder was subjected to multistep testing and laboratory sintering, and the specific surface area after sintering was close to 2 m^2/g. By optimizing channel size, the viscous heat at extremely low temperatures was reduced. Figure 6 shows the SHE developed in this project. At the same time, we have also proposed a convenient and effective numerical method to solve Eqs. (1) and (2), which has enabled us to conduct simulation studies of heat exchangers. The core idea of this numerical solution method is to use constraints to transform the initial value problem of the ODE system into a boundary value problem, which then allows us to employ existing ODE solution modules for resolution. We will soon publish an article dedicated to introducing this numerical solution method and its applications. Furthermore, by combining experimental measurement data, we can evaluate that the E characterizing its Kapitza term for this set of step heat exchangers is around the order of 4.4 (W·K^{-4}·m^{-1}). The local measured values of the heat exchanger temperature, as well as the reverse fitting

values obtained through numerical methods, are illustrated in the Fig. 7. This work provides some theoretical guidance for the evaluation and optimization of our heat exchangers.

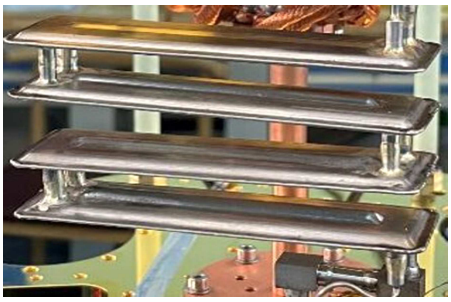


Fig. 6. The stage heat exchanger developed in this project.

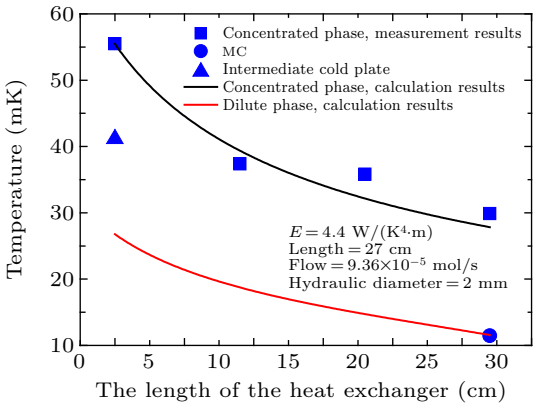


Fig. 7. The temperature distribution of sintered silver powder heat exchanger.

3.4. MC

There is a phase separation interface inside the MC, which is the lowest temperature part of the entire DR. In order to build a usable low-temperature space, it is necessary to transfer the cooling power inside the MC to the cold plate, which also requires overcoming the Kapitza thermal resistance. During the development process, we investigated the effects of several baseplate schemes of MC on the minimum temperature and cooling power of the cold plate experimentally. In the end, we found that optimizing the structural design of the baseplate and the silver powder pressing method can effectively increase the heat transfer area of the MC, thereby reducing the thermal resistance from the liquid interface to the cold plate and improving the effective cooling power of the cold plate. Figure 8 shows the MC developed in this project. Figure 9 shows the equivalent interfacial thermal resistance corresponding to different baseplate schemes. We obtained the thermal resistance by measuring the temperature difference between the inner and outer sides of baseplate under different heating powers. Here, structure 1 represents the bare copper baseplate; structure 2 represents a copper base plate and sintered silver powder with a thickness of 2.5 mm; and structure 3 represents a copper baseplate and sintered silver powder with a thickness of 5 mm. The results of the three structures show the same rule: the lower the temperature, the greater the equivalent interfacial thermal resistance. However, structure 3 shows a better performance near 20 mK.

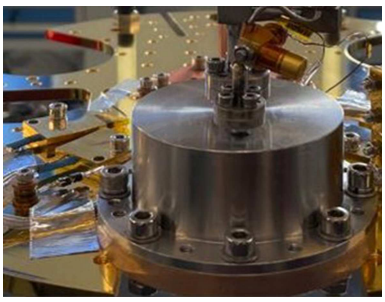


Fig. 8. The MC developed in this project.

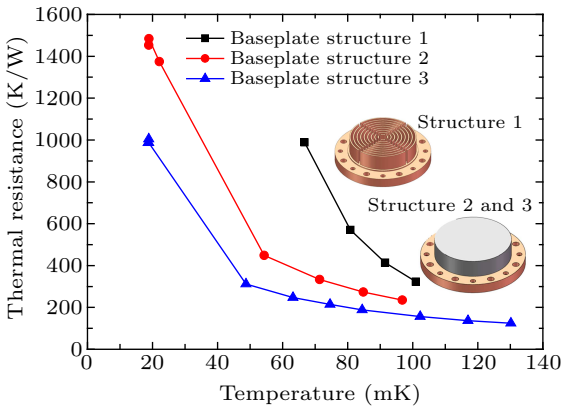


Fig. 9. The interface thermal resistance of different baseplate structures.

4. Experimental results

The prototype of the cryogen-free DR developed in this project is shown in Fig. 10. It is located on the X5 building of the comprehensive extreme condition experimental device at the Institute of Physics, Chinese Academy of Sciences.

After the processes of vacuum pumping, leak detection, precooling, inflation and condensation, the DR can reach its minimum temperature by activating the molecular pump. The cold plate at the MC stage has a diameter of approximately 300 mm, and the lowest temperature it recorded during continuous operation without any external load is 7.6 mK. This temperature was measured by a calibrated ruthenium oxide thermometer from Lakeshore. The DR has maintained continuous operation below 10 mK for over 100 hours. Figure 11 illustrates the temperature variations in the MC when heating power is applied to the heater located on the cold plate. The heating power corresponding to each stable temperature plateau in the figure is 0 μW, 100 μW, 200 μW, 300 μW, 400 μW, and 450 μW, respectively. It is evident that with the application of a 450 μW heating power, the temperature reaches approximately 99.84 mK. Thus, the cooling power of our DR is about 450 μW at 100 mK.

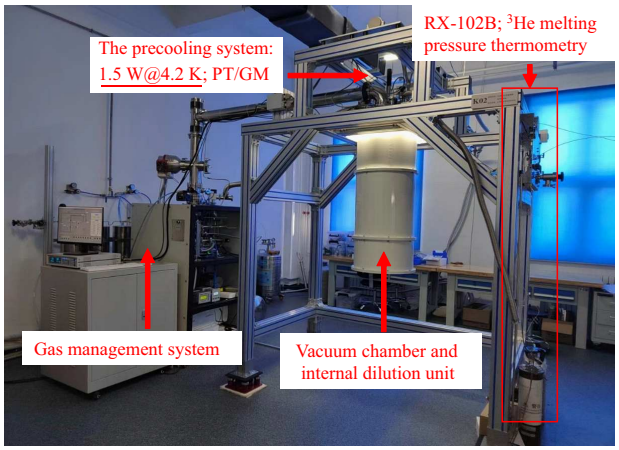


Fig. 10. The cryogen-free DR developed in this project.

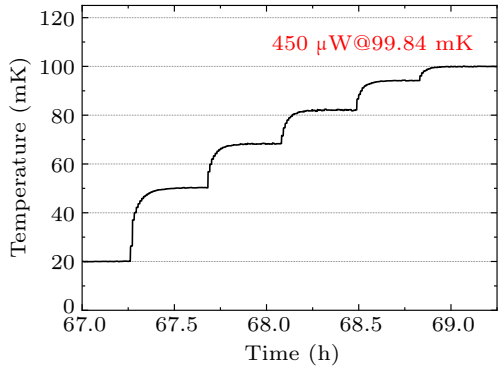


Fig. 11. Test results of cooling power in the MC.

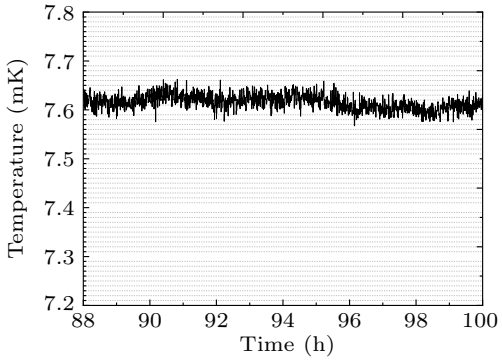


Fig. 12. Temperature fluctuations in the MC during continuous operation.

In addition to the basic temperature, cooling power, and operating time, the prototype developed in this project also exhibits excellent temperature stability. Figure 12 shows the temperature fluctuations of the MC during continuous operation. The measurement results show that the long-term temperature fluctuation is less than 0.1 mK. Figure 13 depicts the overall cooling process of the MC. It can be seen that the system can reach 10 mK within 50 hours. Moreover, we also measured the frequency spectrum of vibration displacement under operating conditions at the room temperature flange, as shown in Fig. 14. The results reveal a vibration peak at 1.78 Hz, which basically corresponds to the vibration frequency of the PT refrigerator. However, in general, within the low-frequency range of interest, the vibration displacement is less than 1 μm.

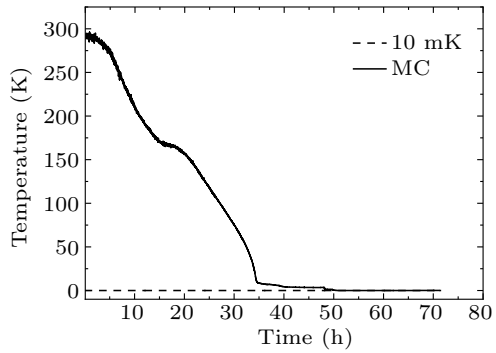


Fig. 13. The cooling process of the MC.

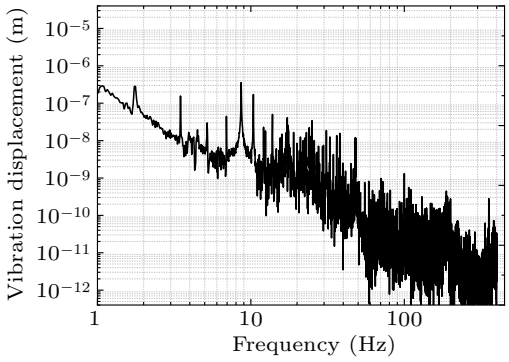


Fig. 14. Vibration measurement results of our DR.

5. Application tests

After completing the development of DR, we also conducted a series of application tests on it, as described in the following subsections.

5.1. Application tests of superconducting quantum computing

The application of quantum computing has the most urgent demand for the development of DR. We have collaborated with the team from the Institute of Physics, Chinese Academy of Sciences to conduct a preliminary application test of quantum computing. Figure 15 displays the quantum computing test platform constructed by the team using the DR we developed, as well as internal photographs of the refrigerator equipped with low-temperature microwave measurement and control cables.



Fig. 15. Quantum computing testing platform (a), and the microwave measurement and control cables installed internally (b).

Table 1. Decoherence and phase cancellation under zero bias frequency.

Qubit	Q1	Q2	Q3	Q4	Q5	Q6	Q7	Q8	Q9	Q10
Frequency (GHz)	4.946	4.986	4.874	5.053	5.078	5.068	4.994	5.12	5.091	5.236
IQ-SNR	10.77	9.42	5.93	8.28	9.13	12.84	9.14	13.77	6.16	8.46
T_1 (μs)/	37.133/	25.545/	28.784/	21.545/	45.783/	38.902/	30.657/	35.061/	36.900/	32.223/
Average T_1 (μs)	29.168	31.019	33.172	34.998	28.585	34.81	32.069	29.326	27.83	26.619
T_{21} (μs)	5.721	5.171	4.92	3.836	5.16	5.609	4.3	5.979	6.034	3.988

In a recent test, the quantum computing team installed a chip[14] integrated with 10 qubits inside the refrigerator, with a total of 21 microwave measurement and control cables. During continuous operation, the minimum temperature of the MC cold plate was 17.24 mK, which meets the experimental requirements of quantum computing. The measurement results indicate that the readout cavities for all qubits were successfully located, with the cavities being deep and exhibiting high quality factors. The signal-to-noise ratio and fidelity for all qubits under zero bias conditions met the expectations. The indicators of energy relaxation time T_1 and phase relaxation time T_2 were good. The detailed test data is shown in Table 1. This experiment was conducted continuously for about 4 months.

5.2. Application tests of low-temperature detector

During the development of this project, we constructed another refrigerator with the same specifications and configurations in parallel, which was used to assist a domestic research institute in conducting experiments with low-temperature detectors. The experiment employed quantum sensor chips and superconducting quantum interference devices to measure radioactive nuclide signals through magnetic calorimetry. Ultimately, the pulse signal from a ^{241}Am radiation source was measured within the temperature range of 20–30 mK, marking China's first breakthrough in this area. Figure 16 displays the refrigerator with a detector chip installed on the cold plate of the MC. Figure 17 shows the raw pulse signal detected by the detector. The execution of this project further confirms the practicality of our DR.

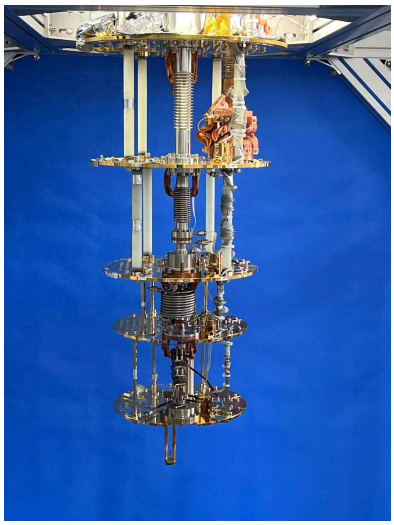


Fig. 16. DR equipped with low-temperature detector chip.

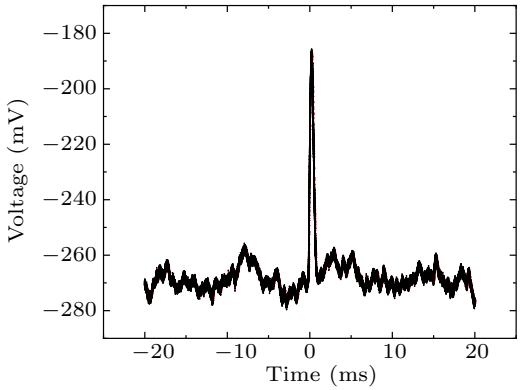


Fig. 17. Original pulse signal detected by detector.

5.3. Magnet integration tests

In the research of condensed matter physics, extreme conditions of low temperature and high magnetic field are widely used, and DRs often need to be equipped with a superconducting magnet to meet the needs of the users. Therefore, we also conducted magnet tests on our cryogen-free DR. In Fig. 18, a set of 8 T magnets is installed with a critical current of 42.16 A. We used the second stage cold plate to cool the magnet located below the MC cold plate by a heat transfer structure. The current leads of the magnet were specially designed and arranged to minimize heat leakage as much as possible. At the same time, a structure to block eddy currents was designed to reduce the impact on the MC. Finally, the magnet could be cooled to a safe temperature of 3.6 K in a natural cooling state. Afterwards, we also conducted a series of tests such as magnetic field scanning (up to 40 A, approximately 7.6 T).



Fig. 18. Cryogen-free DR equipped with magnet.

The magnet achieved the functions expected, while the refrigerator could keep continuous and stable dilution refrigeration in the state of scanning. The temperature rise in the MC caused by eddy currents was less than 5 mK, which was within an acceptable range. This preliminarily verifies the feasibility of the magnet integration scheme.

6. Discussion and improvement

While we have achieved notable strides in the development and application of our equipment, it is important to recognize that there remain areas ripe for exploration and enhancement. Here we list two items.

6.1. Accurate measurement of ultralow temperature

At present, our refrigerator system uses a ruthenium oxide thermometer to measure the temperature in mK range, which belongs to a kind of resistance thermometer with negative temperature coefficient. In addition to the controllable self-heating effect, the resistance thermometer will also be affected by the surrounding microwave heating and external noise. It is particularly important to avoid these disturbances. During the development process, we have measured that the temperature of the concentrated phase solution right before entering the MC (T_{c0}) can reach 24 mK. According to the conclusion that the T_{c0} is about 2.8 times that of the MC (T_{MC}) under zero load, that is, $T_{c0} \approx 2.8T_{MC}$, the T_{MC} should be close to or lower than 10 mK. However, the actual measurement results fluctuate in the range of 12–15 mK, with the change of external shielding conditions. This leads us to infer that the actual lowest temperature should be lower than the reading displayed in the measurement. So, when the refrigerator works in different environments, the grounding and filtering measures may be different, which makes it difficult for us to measure the temperature accurately. Therefore, we believe that a non-resistance thermometer can be used for temperature auxiliary measurement in the future, such as ^{60}Co temperature based on the principle of nuclear orientation. This will further improve the accuracy and reliability of temperature measurement.

6.2. Higher cooling power

A DR with higher cooling power is what we are pursuing in the future. According to

$$Q_{MC} = \dot{n} \cdot (95T_{MC}^2 - 11T_{c0}^2), \tag{3}$$

the cooling power of the MC is directly proportional to the flow of ^{3}He ($\dot{n}$). But the results calculated by Eqs. (1) and (2) show that for a given heat exchanger, the heat exchange effect of the concentrated and dilute phase solution will deteriorate with an increase in flow rate, and then leading to an increase in T_{c0}. Therefore, in order to achieve greater cooling power while ensuring lower temperature, it is necessary to further increase the E value of the heat exchanger, which depends on larger surface area of sintered silver powder or adopting more efficient heat exchange forms. This is also the direction that we are working towards.

7. Conclusion

Building on the technical foundation of our inaugural cryogen-free DR, we have refined the design and manufacturing processes, achieving breakthroughs in some key technologies and components of heat switches and dilution units. Core performance metrics, such as the base temperature and the cooling power at 100 mK, have been improved. Based on this, our DRs have been applied and tested in the fields of quantum computing, low-temperature detectors, and superconducting magnets. Additionally, we have identified potential for further enhancements in temperature measurement accuracy and the development of high-performance ultralow temperature heat exchangers. These efforts are poised to make a meaningful impact in various disciplines, from physics and astronomy to quantum information science.

Acknowledgements

This work was supported by the Beijing Commission of Science and Technology (Grant No. Z211100004021012) and Special Research Assistant Program of the Chinese Academy of Sciences (Grant No. E3VP021RX4). In addition, Dr. Tong Lin, Dr. Jing Dong, and Dr. Guang Yang have also been involved in this work.

References

[1] Zu H Y, Dai W, De Waele A T A M 2022 *Cryogenics.* **121** 103390
[2] IBM scientists cool down the world's largest quantum-ready cryogenic concept system
[3] Hollister Matthew I, Dhuley R C and Tatkowski G L 2022 *IOP Conf. Series: Materials Science and Engineering.* **1241** 012045
[4] Matthew I Hollister, Ram C Dhuley, Christopher James, *et al*. 2023 United States https://www.osti.gov/servlets/purl/1989898.
[5] https://iop.cas.cn/xwzx/snxw/202106/t20210625_6117203.html.
[6] https://www.ahu.edu.cn/2023/0328/c15059a303670/page.htm.
[7] https://mp.weixin.qq.com/s/RnVhacMrma8xJEfWOKnWrA.
[8] https://originqc.com.cn/zh/quantum_control.html?lv2id=44&lv3id=207.
[9] http://www.physike.com/.
[10] Uhlig K 2023 *Cryogenics* **130** 103649
[11] Ji Z, Fan J, Dong J, *et al*. 2022 *Chin. Phys. B* **31** 120703
[12] Poole T, Foster T and Matthews A J 2023 *Cryogenics* **130** 103632
[13] Yan S H and Lu G 1985 *The principles and methods of low-temperature physics experiments* p. 452 (in Chinese)
[14] Li H, Wang Y Y, Shi Y H, *et al*. 2023 *npj Quantum Inf.* **9** 40